Publications of the Astronomical Society of the Pacific
109: 614–627, 1997 May

Night-Sky High-Resolution Spectral Atlas of OH Emission Lines for Echelle Spectrograph Wavelength Calibration. II.[1,2]

DONALD E. OSTERBROCK AND JON P. FULBRIGHT

University of California Observatories/Lick Observatory, Board of Studies in Astronomy and Astrophysics, University of California, Santa Cruz, California 95064
Electronic mail: don@ucolick.org, jfulb@ucolick.org

THOMAS A. BIDA

W. M. Keck Observatory, California Association for Research in Astronomy, Kamuela, Hawaii 96743
Electronic mail: tbida@keck.hawaii.edu

Received 1996 November 15; accepted 1997 January 20

ABSTRACT. The potential of night-sky emission lines recorded on every long-exposure astronomical spectrum, for wavelength calibration, is reemphasized. The previously published high-resolution atlas, based on spectra obtained with the Keck 10-m telescope on Mauna Kea and the HIRES high-resolution echelle spectrograph, is extended from 9000 to 10,600 Å, the present effective long-wavelength limit for reasonable exposure times with current CCDs. The extension of the atlas shows many OH night-sky lines, and makes it possible to identify them easily on high-resolution spectra. Accurate wavelengths and references to their sources are given. Measured intensity ratios for the resolved, well-measured lambda-type doublets are presented, and the probable errors in the listed wavelengths of the unresolved doublets, based on them, are discussed. Observations and identifications of a number of lines of weak satellite or intecombination bands of OH in the night-sky spectrum are discussed, and the "not proven" result of a search for OH lines in the $(10 - 5)$ and $(10 - 4)$ bands is mentioned.

1. INTRODUCTION

The numerous OH emission lines of the night-sky spectrum, although they contaminate every observed spectrum of a star, nebula, or galaxy, also provide a potentially useful wavelength-calibration spectrum taken automatically as a byproduct of that exposure. For high-resolution spectra, these OH lines are particularly appropriate because their laboratory wavelengths have been very accurately measured and published (Abrams et al. 1994), and because they are well distributed through the yellow, red, and infrared spectral regions. Thus at least a few of them appear in every order of high-resolution echelle spectrographs like the HIRES spectrograph on the Keck 10-m telescope (Vogt et al. 1994). To identify the OH lines on a spectrum an atlas in which the strongest lines are marked and hence instantly recognizable is very useful. Hence two of us, with several other collaborators, published such an atlas, based on then-available spectra, extending over the spectral range λλ5190– 8990 (Osterbrock et al. 1996, hereafter Paper I). In the present paper, based on more recently obtained spectra, we extend this atlas to λ10600, which is about the long-wavelength limit of currently available CCDs with reasonable exposure times.

[1]Lick Observatory Bulletin 1351.
[2]Based on observations obtained at the W. M. Keck Observatory, which is operated by the California Institute of Technology and the University of California.

2. OBSERVATIONAL DATA

The extension of the atlas to longer wavelengths contained in the present paper is based on two pairs of exposures of the night sky taken with HIRES by Bida, as listed in Table 1. "Left" and "right" are two different echelle settings, as explained in Paper I. The night-sky spectra were extracted from these exposures and were combined to provide complete spectral coverage from λ8795 to λ10600 (echelle orders 40 through 34) for this paper. Note that order 40 is included in Paper I and in this one, but with somewhat different central wavelengths, so that there are no gaps in the coverage between orders in either paper. In the present paper the resulting night-sky spectrum extends from λ8790 (in order 40) to λ10600 (in order 34). As in Paper I the slit widths were chosen to give a resolution ~ 0.2 Å at λ7000, while the dispersion at the CCD was 0.05 Å pix^{-1}, so the spectra were well sampled.

The wavelength scale was calibrated from the OH lines themselves, as described in Paper I, and the individual orders are plotted in Figs. 1 through 7. As in that paper the continuum was flattened and nearly entirely removed, and the intensity scale for each order was normalized so that its strongest line peaks at 1.00. Thus each order is plotted at a different intensity scale, and the noise level therefore differs from one order to the next. The noise also increases toward longer wavelength because of the decreasing sensitivity of the CCD. This atlas provides a good starting point for identifying night-sky lines in this spectral region which are likely to be recorded with currently available CCDs and exposure

TABLE 1
Journal of Night-Sky-Spectra Observations

	Shorter Wavelength		Longer Wavelength	
	left	right	left	right
Observer	Bida	Bida	Bida	Bida
Date	11 Jan 1996	10 Sep 1995	11 Jan 1996	11 Jan 1996
UT	5:52	10:18	6:14	6:30
Orders	36–47		30–36	
$\lambda\lambda$	7476–10035		9760–11990	
Exposure	25 min.	20 min.	15 min.	15 min.
α (1950)	00^h25^m	00^h52^m	00^h25^m	00^h25^m
δ (1950)	$+04°47'$	$+45°00'$	$+04°47'$	$+04°47'$
Zenith Distance (°)	39	33	44	48
Azimuth (°)	250	13	255	257

times comparable to those most observers on the Keck HIRES spectrograph use.

3. OH BANDS

All of the night-sky lines we identified in this spectral region are from the Meinel rotation-vibration bands of OH. Very accurate laboratory wavelengths for this band system have been measured and published by Abrams et al. (1994). Hence in the figures we label the OH lines by their designations in the standard spectroscopic notation used by these authors, and give the wavelength to 0.001 Å from their Table 29 (in which they are given to their full accuracy, 0.00001 Å). The standard spectroscopic notation, described by Herzberg (1950), is briefly summarized in the context of the OH Meinel bands in Paper I. As in that paper, the straight arithmetic mean of the wavelengths of the two components, e and f, is shown in the figures for all pairs in which the Λ-type doubling is smaller than 0.2 Å, about the effective limit of resolution for the Keck HIRES with the slit width commonly used, while the wavelengths of the individual components are shown for pairs with splitting larger than this limit. Furthermore, if two lines are separated by 0.1 Å or less, the mean wavelength is marked with an asterisk as in Paper I. As stated there, the best lines to use for wavelength calibration are the single lines marked with an e or an f in the figures. The next best are the blends with separation less than 0.1 Å, marked with an asterisk. Their mean wavelengths could be very slightly in error, if their e and f components differ greatly in intensity, as discussed in more detail in Sec. 4. The least desirable lines to use are blends with separations between 0.1 and 0.2 Å; they are not marked with either an asterisk or e or f on the figures. Since their separations are larger, the errors in their mean wavelengths could be proportionately larger.

In their Table 29, Abrams et al. list wavelengths of $P(J)$ and $Q(J)$ lines with $J \leq 4.5$, and of $R(J)$ with $J \leq 3.5$. For the many lines of higher J which we have identified in the OH night-sky spectrum, we have calculated the wavelengths using the energy levels deduced from their laboratory data by Abrams et al. (1994) and published in their Table 27. For the conversion from vacuum to air wavelengths we used the dispersion formula for standard air of Edlén (1953), the same one used by Abrams et al. These wavelengths are on exactly the same system as those published in their paper, and differ at most by 0.0001 Å from the air wavelengths calculated with the later dispersion formula of Edlén (1966). The lines of high J are especially useful for wavelength calibration, because their large Λ-type doubling clearly resolves the e and f components.

For completeness, these calculated wavelengths for the higher-J lines clearly observed in the night-sky spectrum in the interval 9000 Å $\leq \lambda \leq$ 10,500 Å are listed in Table 2. They are entered in the figures in the same way as the lines listed by Abrams et al. for lower J. The calculated wavelengths for the higher rotational lines with $\lambda \leq 9000$ Å were previously published in Table 2 of Paper I.

4. DOUBLET INTENSITY RATIOS

As stated in Paper I, the intensities of the two components of each OH line, split by Λ-type doubling, are expected to be equal under the simplifying assumption of thermodynamic equilibrium. For this reason, the straight mean wavelength of all pairs which are not resolved has been adopted in this paper and in Paper I. To test this assumption we have measured the relative intensities of all the resolved pairs which have good signal-to-noise-ratio (S/N>50) in our summed spectra of Paper I and this paper. The results, in the form of intensity ratios I_e/I_f, are presented in Table 3. For these relatively strong lines the major source of error in the measured ratios seems to be the noise in the "continuum," which is probably a mixture of scattered moonlight, zodiacal light, background stars, and galaxies. All these sources have absorption lines in their spectra, which simulate noise; no doubt much of it could be considerably reduced if sufficient observing time were available. We have estimated the probable error σ in each measured intensity ratio by sketching in alternate straight lines which could conceivably be used to represent the continuum, and reducing the measurements made with them as well. The resulting probable errors are listed in the last column in Table 3. Typically, the lines with S/N $\geq$ 60 have $\sigma \leq 0.02$, and those with S/N $\geq$ 30 have $\sigma \leq 0.03$.

It can be seen that 21 of the measured intensity ratios differ from the expected value 1.00 by more than the prob-

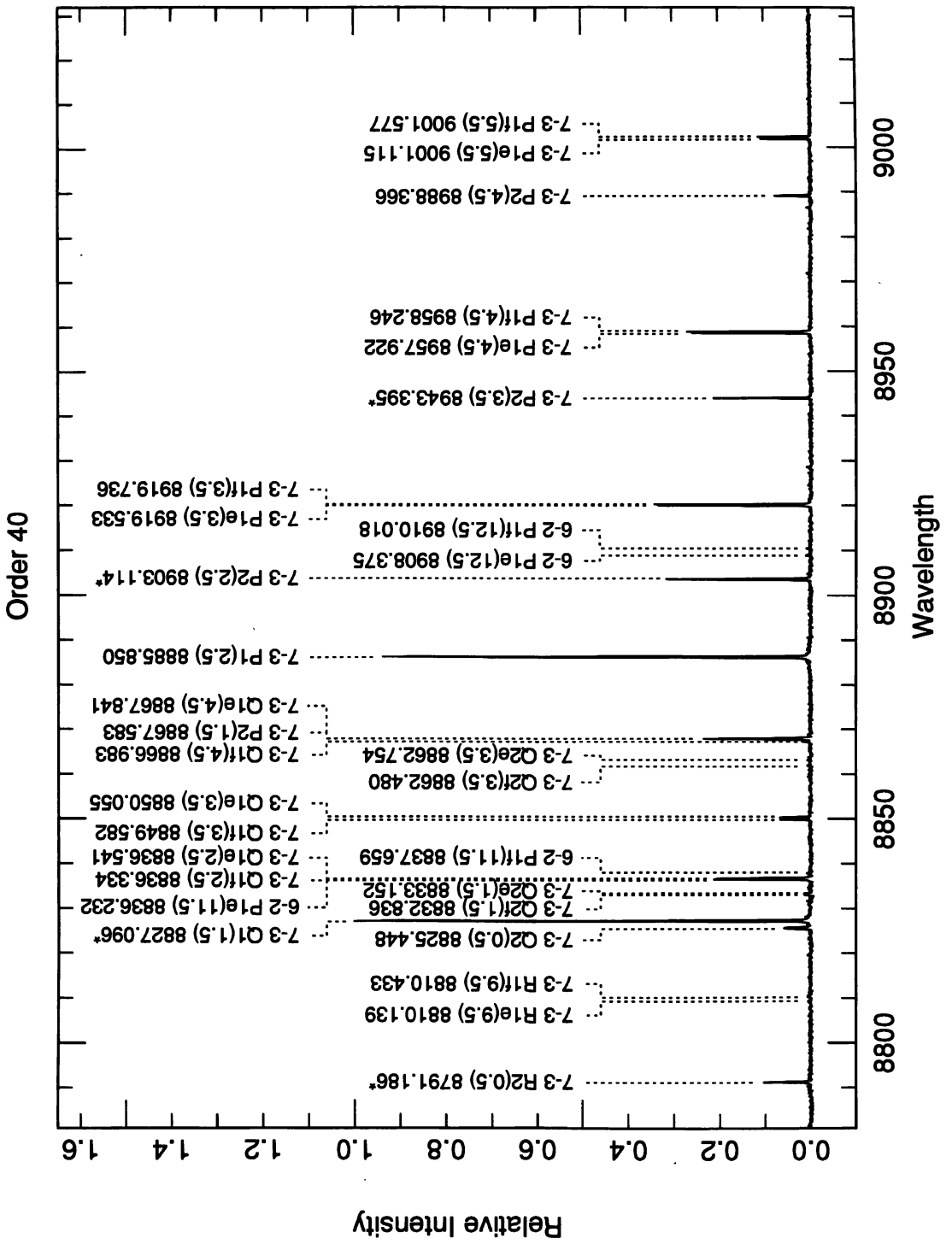

FIG. 1—Order 40 of Mauna Kea night-sky emission-line spectrum.

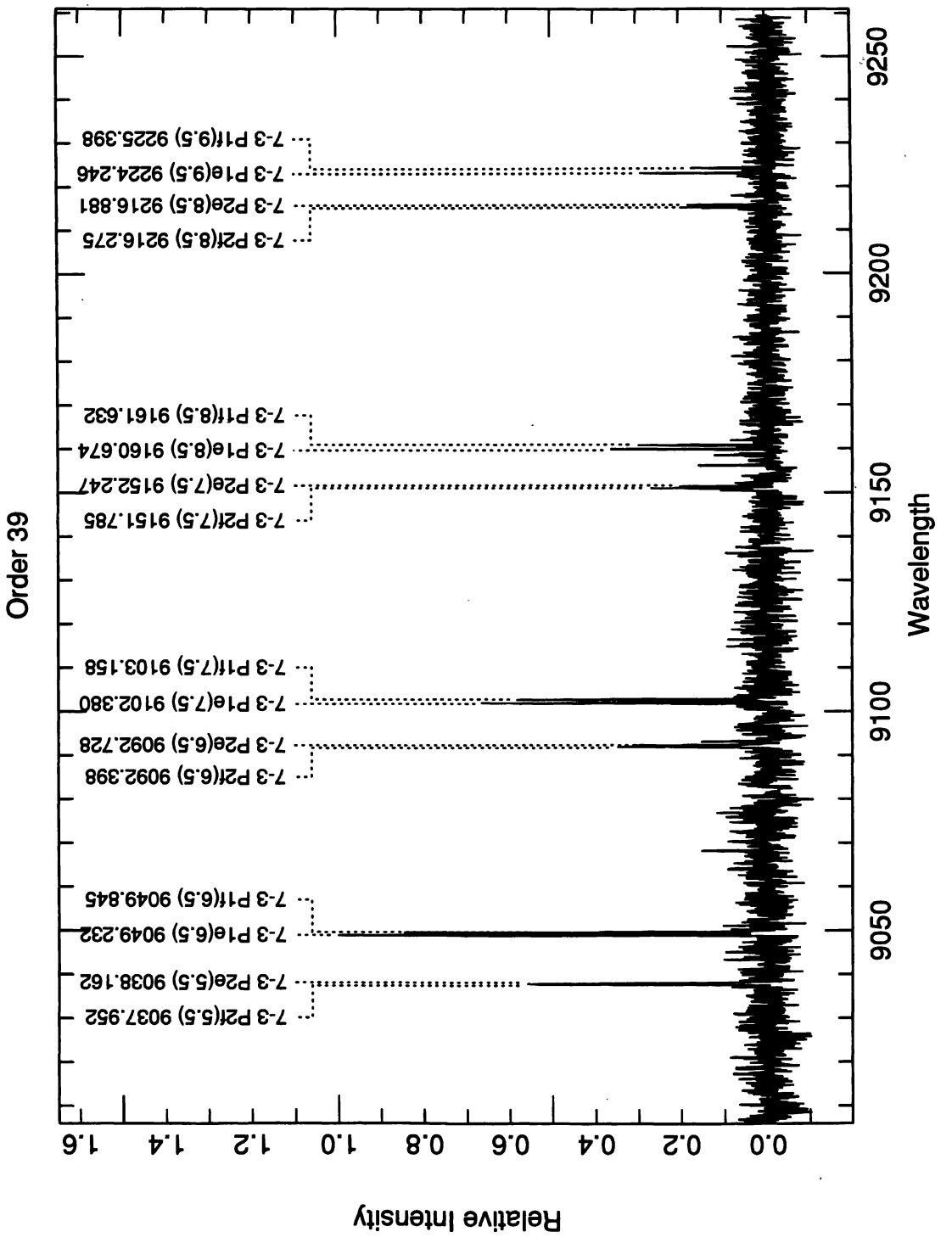

FIG. 2—Order 39 of Mauna Kea night-sky emission-line spectrum.

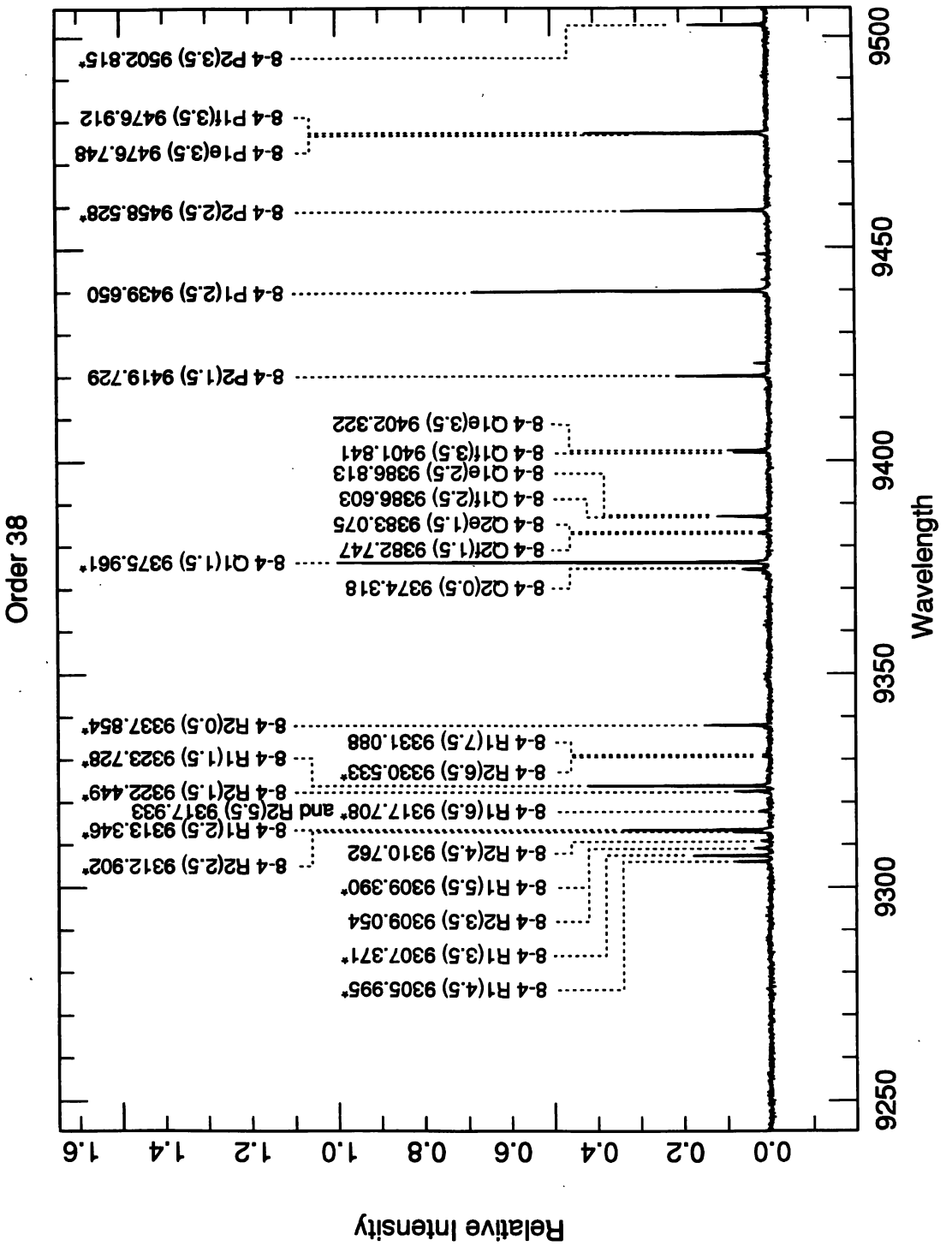

FIG. 3—Order 38 of Mauna Kea night-sky emission-line spectrum.

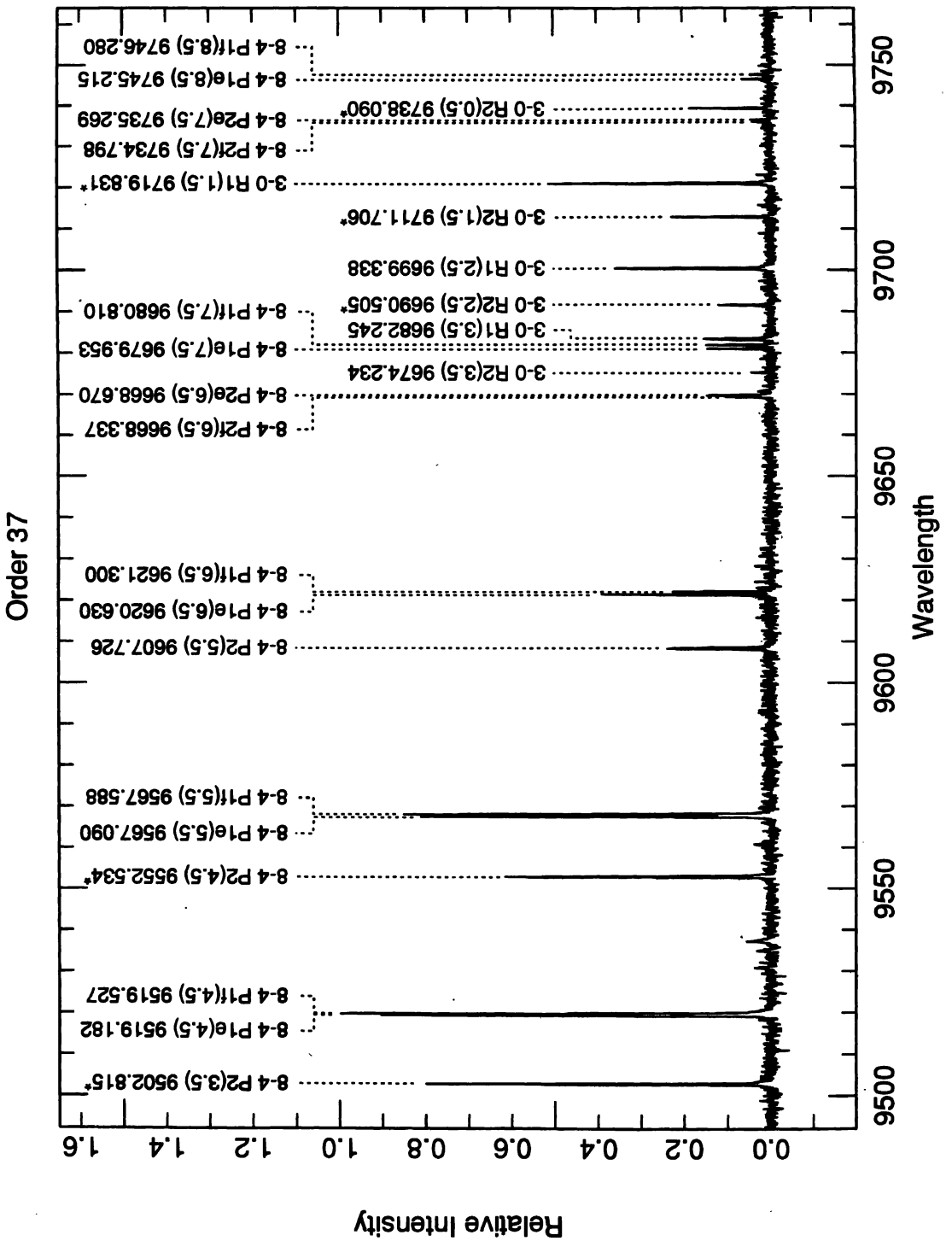

FIG. 4—Order 37 of Mauna Kea night-sky emission-line spectrum.

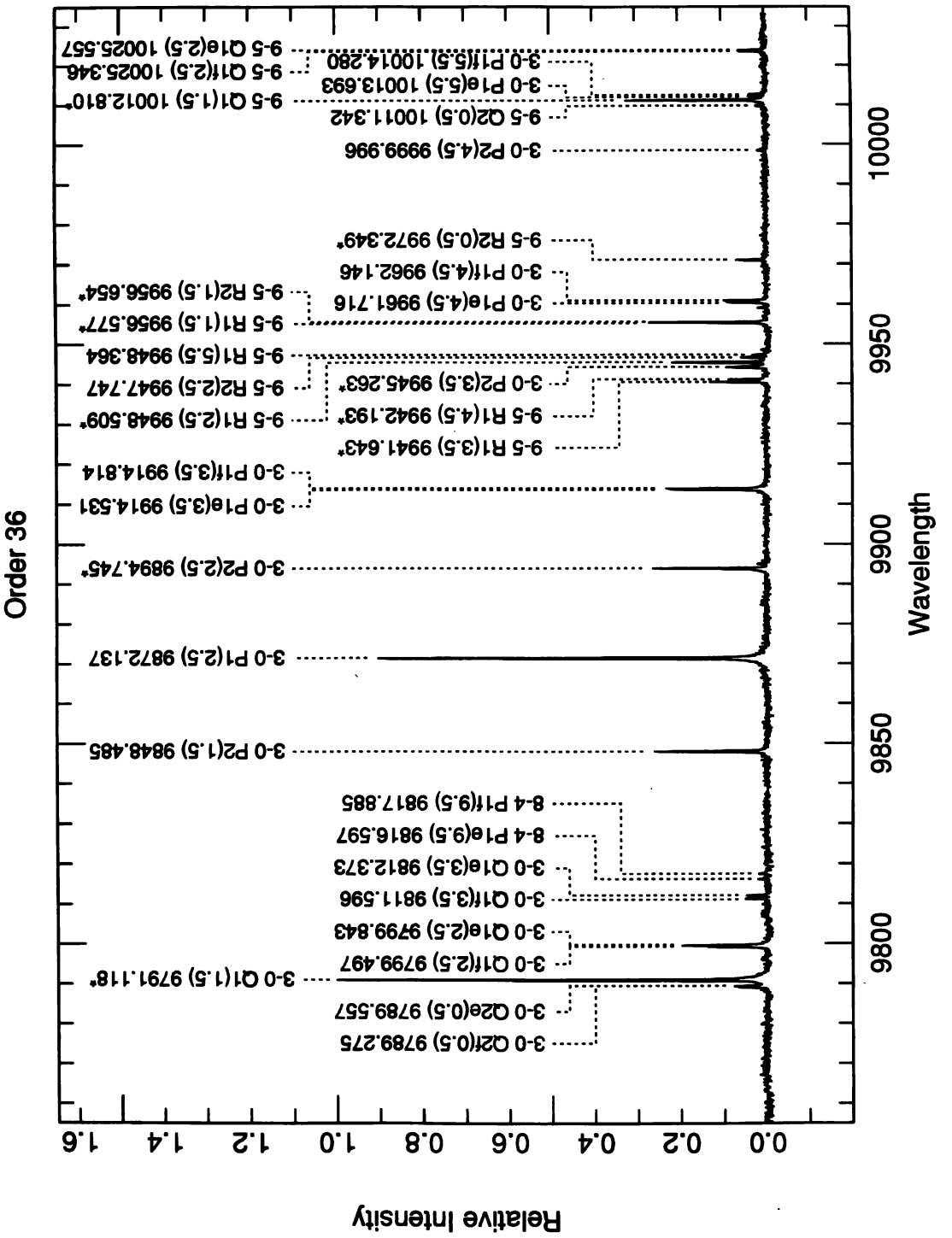

FIG. 5—Order 36 of Mauna Kea night-sky emission-line spectrum.

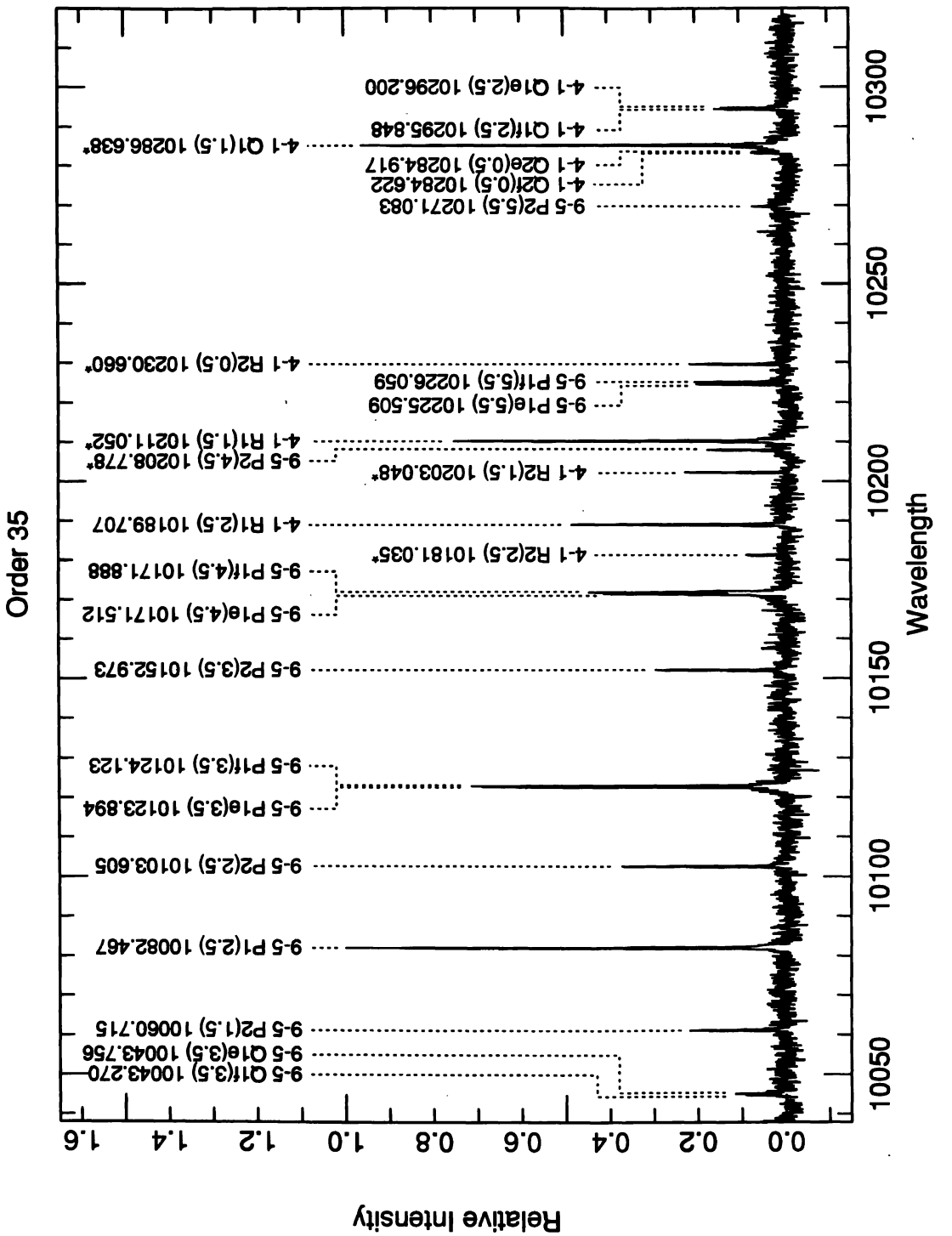

FIG. 6—Order 35 of Mauna Kea night-sky emission-line spectrum.

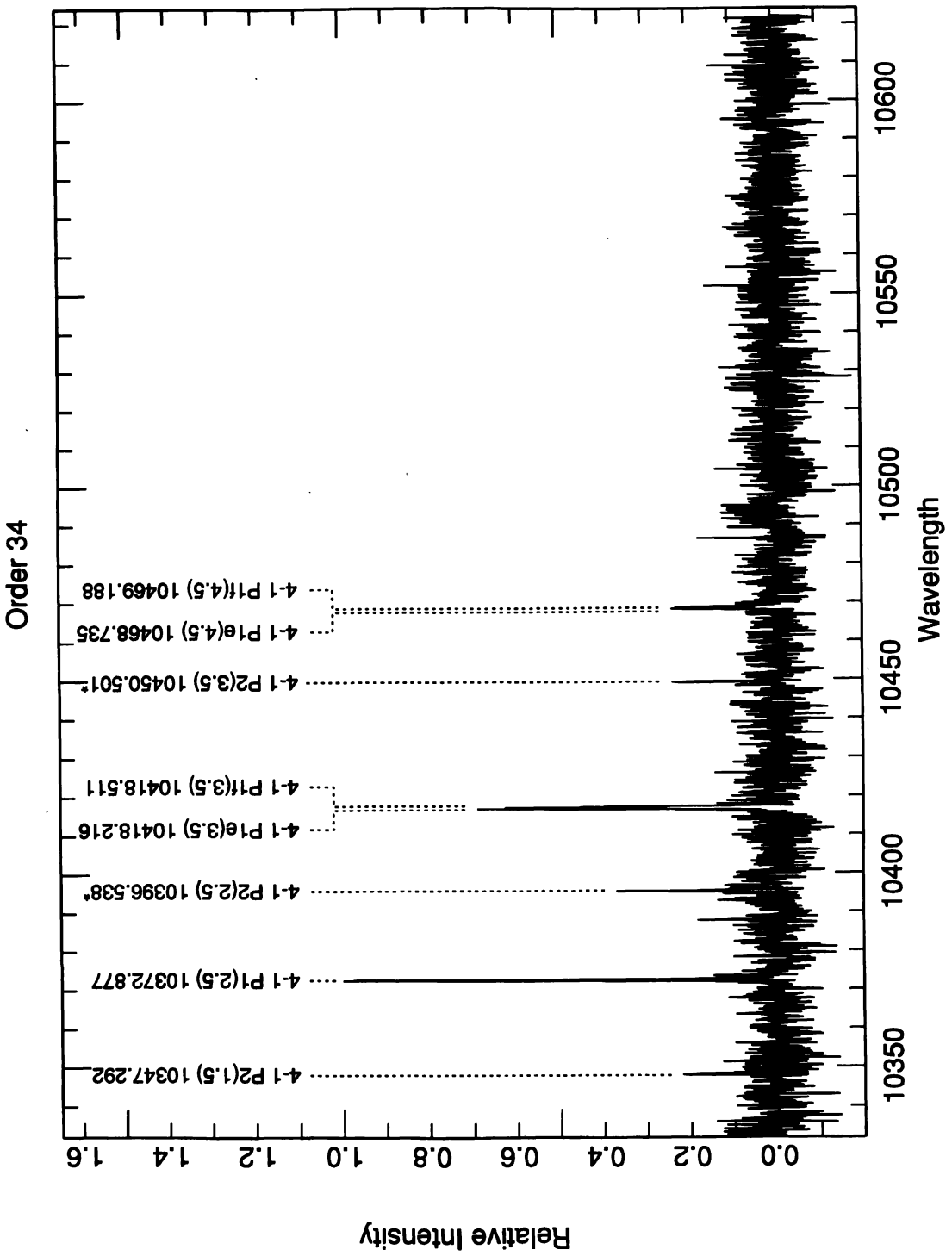

FIG. 7—Order 34 of Mauna Kea night-sky emission-line spectrum.

TABLE 2
Observed OH Lines Not Listed in Abrams et al. (1994)

v'-v"	Identificaion	Wavelength	v'-v"	Identificaion	Wavelength
7-3	P1e(5.5)	9001.115	8-4	R1e(7.5)	9330.999
7-3	P1f(5.5)	9001.577	8-4	R1f(7.5)	9331.178
7-3	P2f(5.5)	9037.952	8-4	P1e(5.5)	9567.090
7-3	P2e(5.5)	9038.162	8-4	P1f(5.5)	9567.588
7-3	P1e(6.5)	9049.232	8-4	P2f(5.5)	9607.625
7-3	P1f(6.5)	9049.845	8-4	P2e(5.5)	9607.828
7-3	P2f(6.5)	9092.398	8-4	P1e(6.5)	9620.630
7-3	P2e(6.5)	9092.728	8-4	P1f(6.5)	9621.300
7-3	P1e(7.5)	9102.380	8-4	P2f(6.5)	9668.337
7-3	P1f(7.5)	9103.158	8-4	P2e(6.5)	9668.670
7-3	P2f(7.5)	9151.785	8-4	P1e(7.5)	9679.953
7-3	P2e(7.5)	9152.247	8-4	P1f(7.5)	9680.810
7-3	P1e(8.5)	9160.674	3-0	P2f(7.5)	9734.798
7-3	P1f(8.5)	9161.632	3-0	P2e(7.5)	9735.269
7-3	P2f(8.5)	9216.275	3-0	P1e(8.5)	7945.215
7-3	P2e(8.5)	9216.881	3-0	P1f(8.5)	9746.280
7-3	P1e(9.5)	9224.246	8-4	P1e(9.5)	9816.597
7-3	P1f(9.5)	9225.398	8-4	P1f(9.5)	9817.885
8-4	R1f(4.5)	9305.982	9-5	R1e(4.5)	9942.189
8-4	R1e(4.5)	9306.009	9-5	R1f(4.5)	9942.197
8-4	R2e(4.5)	9310.701	9-5	R1e(5.5)	9948.327
8-4	R2f(4.5)	9310.822	9-5	R1f(5.5)	9948.402
8-4	R1e(6.5)	9317.663	3-0	P1e(5.5)	10013.693
8-4	R1f(6.5)	9317.753	3-0	P1f(5.5)	10014.280
8-4	R2e(5.5)	9317.878	9-5	P1e(5.5)	10225.509
8-4	R2f(5.5)	9317.988	9-5	P1f(5.5)	10226.059
8-4	R2e(6.5)	9330.493	9-5	P2f(5.5)	10270.990
8-4	R2f(6.5)	9330.574	9-5	P2e(5.5)	10271.175

able error, while eight differ from it by less than the probable error. Thus it appears that there are real deviations from the expected value 1.00 for some of these line ratios. Presumably they occur through whatever mechanisms populate the individual e and f levels of OH; if the downward radiative transition probabilities are truly independent of this symmetry property, as expected on very general principles, the difference must occur in the original formation process of the OH molecules, believed to be a two-body reaction involving O_3 and atomic H. This possibility has been discussed in some detail by Dodd et al. (1994). In no case have we been able to measure accurately an I_e/I_f ratio for a $P_1(J'')$ and a $Q_1(J'')$ with the same upper level J', which would distinguish between the population and the downward radiative transition probability as the cause of the deviation of the intensity ratio from unity. The problem is that the intensities of the $Q_1(J)$ lines decrease rapidly with increasing J, while the $P_1(J)$ splitting is too small to resolve the individual components at small J. Much longer exposure times could solve this problem.

A conceivable source of error in the measured I_e/I_f could be partial absorption of OH emission lines by atmospheric H_2O or O_2 (Espy and Hammond 1995). Given the thermal Doppler widths of the OH emission lines with T = 200–300 K, 0.02 Å as measured by Greet et al. (1994), and the somewhat broader H_2O (0.06 Å) and O_2 (0.04 Å) lines, as estimated from a high-resolution solar atlas (Delbouille et al. 1973), this would require coincidence of the emission and absorption lines to 0.05 Å or less. Of the 58 OH lines measured and listed in Table 3, none is closer than 0.04 Å to an atmospheric absorption line listed in the solar spectrum by Moore et al. (1966). In fact, the two OH emission lines closest to telluric absorption lines are (8-3) $P_{1e}(4.5)\lambda 7369.248$, which is 0.04 Å from atmospheric $H_2O\lambda 7369.206$, and (4-0) $P_{1e}(5.5)\lambda 7662.175$, which is 0.05 Å from the atmospheric O_2 line $\lambda 7662.12$. In both cases the potentially partly absorbed P_{1e} component was measured to be stronger, not weaker, than the corresponding P_{1f} component. There are only two other measured OH lines in Table 3 closer than 0.10 Å to a listed atmospheric absorption line, and only six more closer than 0.20 Å. Most of them are H_2O lines, and the great majority are very weak or do not show at all in the solar spectral atlas, observed at the Jungfraujoch at 3576 m altitude, while Mauna Kea, at 4215 m, is even higher and drier. Thus this potential alternate interpretation of deviation of the measured I_e/I_f intensity ratios from 1.00 seems to be untenable.

Whatever the source of the deviation of I_e/I_f from 1.00, it affects the measured wavelengths of the blended lines made up of the two components. If it is correct to assume that the measured wavelength of the blend is the intensity-weighted average of the wavelengths of the two components, then

TABLE 3
Intensity Ratios of Resolved Lambda-Type Doublets

Band	Line	Wavelength	I_e/I_f	σ
9-4	P1(7.5)	7977	1.02	0.07
	P1(5.5)	7890	0.96	0.02
	P1(4.5)	7853	0.94	0.01
	Q1(3.5)	7773	0.93	0.04
9-3	P1(8.5)	6458	0.97	0.08
	P1(7.5)	6420	1.11	0.09
8-3	P1(9.5)	7574	1.11	0.08
	P1(7.5)	7479	1.08	0.02
	P1(6.5)	7438	1.13	0.02
	P1(5.5)	7402	1.05	0.02
	P1(4.5)	7369	1.04	0.01
	Q1(3.5)	7296	0.94	0.02
7-3	P1(5.5)	9001	1.00	0.03
	P1(4.5)	8958	0.97	0.01
	Q1(3.5)	8850	0.96	0.02
7-2	P1(6.5)	7011	1.09	0.02
	P1(5.5)	6878	1.06	0.01
	Q1(3.5)	6881	0.95	0.02
6-2	P1(7.5)	8597	1.04	0.03
	P1(6.5)	8549	1.07	0.03
	P1(5.5)	8505	1.05	0.01
	P1(4.5)	8465	1.14	0.02
	Q1(3.5)	8365	1.04	0.04
6-1	P1(5.5)	6604	1.03	0.02
5-1	P1(6.5)	8102	1.00	0.03
	P1(5.5)	8062	1.04	0.02
	P1(4.5)	8026	1.03	0.01
4-0	P1(5.5)	7662	1.02	0.06
	Q1(3.5)	7540	0.96	0.07

$$\langle\lambda\rangle=\frac{\lambda_1+\lambda_2}{2}+\frac{(i-1)}{(i+1)}\times\frac{\Delta}{2},$$

where

$$i=\frac{I_2}{I_1}$$

is the intensity ratio of the two components, and

$$\Delta=\lambda_2-\lambda_1$$

is the separation between them.

If the median measured intensity ratio of Table 3, $i = 1.03$, also represents a "typical" value for the unresolved lines of smaller J, and if we take $\Delta = 0.15$ Å as a typical separation of the "least-desirable" lines of this type to use for wavelength calibration, the "typical" error in using the mean wavelengths tabulated in Table 2 of this and our previous paper, is 0.002 Å. For $i = 1.14$, the extreme measured intensity ratio of Table 3, and $\Delta = 0.20$ Å, the "extreme" error is 0.012 Å. This illustrates the advantage of using resolved OH lines for wavelength calibration whenever possible, and if this is impossible, of measuring several unresolved blends in each order, to average out such uncertainties. Of course, we have not measured the intensity-ratio i for any unresolved blends, and the above discussion depends, as stated, on the assumption that the ratios measured for the lines of higher J are indicative of those of lower J as well.

5. FAINT OH LINES

The OH night-sky emission lines are of great interest in atmospheric research, and our HIRES scans combine unusually high spectral resolution and wide-wavelength coverage. Most previous night-sky observational research at comparable resolution has been done with Fabry–Perot interferometers. Taken as our spectral scans were at Mauna Kea, a low-latitude site, they are free of auroral "contamination," and allow the night-sky spectrum to be studied in relatively pure form. In this and the next section we therefore discuss some of the weaker features which, although they are not directly useful for astronomical wavelength calibration, are informative for atmospheric research. The measurements discussed here are based on the spectral scans of Paper I and the present paper, mostly the former, which combine greater CCD sensitivity and longer exposure times.

Several of the observed OH bands, particularly the P_1 bands, can be followed to quite large J in the wavelength regions in which the bands are strong, the CCD sensitivity is high and we have good long-exposure data. To show this quantitatively, in Table 4 we have listed the largest J easily detectable on our scans. The maximum intensities of the various P_1 and P_2 bands occur around $J = 2.5$, corresponding to rotational temperature $T \approx 150$–200 K in the emitting regions (see, e.g., Rees 1989; Greet et al. 1994; Taylor et al. 1995; Williams 1996), but the observed intensities of these highest J lines appear to be larger than expected for such a thermal distribution. They therefore tend to confirm that the highest J levels have non-LTE populations, perhaps as a result of the processes by which the OH molecules are formed (Pendleton et al. 1989). Well-calibrated spectra, taken with HIRES or the fairly similar, but not quite as advanced, Hamilton spectrograph (Vogt 1987) at Lick Observatory could make this comparison quantitatively.

It is also of interest to use these sky spectra to see if it is possible to detect any weak OH emission lines from bands with upper vibrational quantum number $v' = 10$. All the night-sky OH lines reported and generally accepted to date are from levels $v' \leq 9$, which is interpreted as meaning that the formation process does not provide enough excess energy to excite still higher vibrational levels. However, it is conceivable that some weak secondary process may surmount this threshold. Some years ago Krassovsky et al. (1961, 1962) reported observing the (10–4) $Q_1(1.5)$ λ6688.5 line and the (10 − 4) R_1 head at λ6664 in the night-sky spectrum, but the evidence seemed weak. Abrams et al. (1994) did observe the (10–9) and (10–8) OH bands in the laboratory, determined the rotational energy levels from $v' = 10$, and listed the calculated wavelengths for the (10 − 4), (10 − 5), and (10 − 6) bands in their Table 29. In the spectral region for which we have data, the best possibilities for detection are the strongest lines of the (10 − 5) bands. In the analogous observed (9 − 4) bands in the night-sky spectrum, the strongest features are the

TABLE 4
Maximum J'' Observed in Each Band

Δv	$v' - v''$	Bandhead	R_1	R_2	P_1	P_2	Q_1	Q_2
7	9-2	5187	—	—	4.5	—	1.5	1.5
6	6-0	5254	2.5	1.5	—	—	—	—
	7-1	5542	2.5	1.5	5.5	5.5	2.5	0.5
	8-2	5862	3.5	3.5	8.5	6.5	2.5	0.5
	9-3	6234	5.5	2.5	8.5	7.5	3.5	2.5
5	5-0	6137	5.5	1.5	5.5	4.5	3.5	—
	6-1	6464	4.5	3.5	10.5	7.5	3.5	0.5
	7-2	6827	7.5	6.5	14.5	13.5	4.5	1.5
	8-3	7239	6.5	5.5	11.5	10.5	4.5	1.5
	9-4	7712	6.5	5.5	9.5	8.5	4.5	1.5
4	4-0	7461	5.5	3.5	6.5	6.5	4.5	1.5
	5-1	7849	5.5	4.5	18.5	15.5	4.5	1.5
	6-2	8278	10.5	9.5	13.5	12.5	4.5	1.5
	7-3	8759	9.5	3.5	9.5	8.5	5.5	3.5
	8-4	9306	7.5	6.5	9.5	7.5	3.5	1.5
	9-5	9942	5.5	2.5	5.5	5.5	3.5	0.5
3	3-0	9652	3.5	3.5	5.5	4.5	3.5	0.5
	4-1	10143	2.5	2.5	4.5	3.5	2.5	0.5

$R_1(1.5\text{–}4.5)$ lines between λλ7712–7717, followed by the somewhat weaker $Q_1(1.5)$, and the still weaker $P_1(2.5)$. We searched for the (10 − 5) $Q_1(1.5)$ λ8308.37, and found a weak, otherwise unidentified line with λ8308.40. It is roughly the same strength as the neighboring (5 − 1) $P_{1f}(10.5)$ λ8305.18, about 0.005 the strength of (6−2) $Q_1(1.5)$, or two-thirds as strong as (5−1) $P_{1e}(10.5)$ λ8304.07, although there are features indistinguishable from noise at some of these wavelengths. However, we did not find any lines corresponding to (10 − 5) $R_1(1.5,2.5,3.5)$ λλ8272.07, 8268.60, 8269.78, nor to (10 − 5) $P_1(2.5)$ λ8356.28. The OH (10 − 4) bands are less favorable on our spectra, because they are in a noisier region. Nevertheless, we searched for $Q_1(1.5)$, $R_1(1.5)$, and $P_1(2.5,3.5)$, all without success. Two of these are the features reported as present in the night-sky spectrum (over Yakutsk rather than Hawaii) by Krassovsky et al. The (10 − 6) bands centered on $Q_1(1.5)$ λ10770.36 lie in an even noisier region on our spectra, not worth searching carefully. The single probable identification of (10 − 5) $Q_1(1.5)$ by itself is tantalizing, but not sufficient to provide convincing evidence for OH molecules with $v' = 10$ in the night sky over Mauna Kea. Still longer exposures, yielding better signal-to-noise ratio spectra in the region of the (10 − 5)R_1 head, will be necessary to settle this question.

6. SATELLITE OH BANDS

In addition to the main P_1, P_2, Q_1, Q_2, R_1, and R_2 OH bands, which occur under the selection rules applying in Hund's case (a) as described in Paper I, six additional types of bands can occur under case (b). The OH $^2\Pi_{3/2,1/2}$ electronic states are close to case (a), particularly in their lower rotational levels, but approach case (b) at large J. Hence weak "satellite" or "intercombination" bands of this type are expected to occur at some nonzero intensity as well. These bands all involve transitions between the two electronic states. The selection rules for them, given in Herzberg (1950), are as follows:

$$^{Q}R_{12}: J' - J'' = +1,\ K' - K'' = 0,$$

$$^{R}Q_{21}: J' - J'' = 0,\ K' - K'' = +1,$$

$$^{P}Q_{12}: J' - J'' = 0,\ K' - K'' = -1,$$

$$^{Q}P_{21}: J' - J'' = -1,\ K' - K'' = 0,$$

$$^{O}P_{12}: J' - J'' = -1,\ K' - K'' = -2,$$

$$^{S}R_{21}: J' - J'' = +1,\ K' - K'' = +2.$$

Thus the selection rules for J (and also those for e and f, not listed here) are identical with those for the corresponding main R, Q, and P bands, but $\Delta K = \Delta J \pm 1$ for the satellite bands instead of $\Delta K = \Delta J$ as for the main bands. In the designations of the satellite bands the first number in the subscript stands for the upper electronic level of the transition and the second for the lower electronic level, with $1 = {}^2\Pi_{3/2}$ and $2 = {}^2\Pi_{1/2}$.

To the best of our knowledge, no lines of these satellite or intercombination bands of OH $^2\Pi - {}^2\Pi$ have been observed in the laboratory. Two weak features have been identified in the night-sky spectrum, both in the (3 − 1) band, $^{P}Q_{12}(1.5)$ at 6456.4 cm^{-1} and $^{Q}R_{12}(0.5)$ at 6515.1 cm^{-1} by Turnbull and Lowe (1983) from their Fourier transform spectrometer measurements. More recently Greet et al. (1997) reported identifications of the (6 − 2) $^{Q}R_{12}(1.5 + 2.5)$ λ8427.6 blend, the $^{Q}R_{12}(0.5)$ λ8434.4 line, and the $^{P}Q_{12}(1.5)$ λ8427.6 line from their spectral scans obtained with a Czerny–Turner grating spectrometer operating in the first order.

In our night-sky spectra we have identified many more of these satellite lines, by measuring the wavelengths of the faint lines in the region with the best signal-to-noise ratio. The strongest are all in the $^{Q}R_{12}$, $^{P}Q_{12}$, and $^{O}P_{12}$ bands, just as the main R_1, Q_1, and P_1 bands are stronger than R_2, Q_2, and P_2, because of the higher population in the $^2\Pi_{3/2}$ ground electronic level. Typically, these strongest satellite lines have intensities in the range 0.01–0.03 of the strongest lines in the main bands of the same vibrational transition. We calculated the predicted wavelengths using the energy levels published by Abrams et al. (1994) in exactly the same way as the wavelengths of the main-band lines of high J, as described in Sec. 3. The OH satellite lines identified in our night-sky spectrum in this way are listed in Table 5. If two satellite lines may possibly be blended, they are given in successive lines in the calculated wavelength and identification columns, with the first of these blended lines tabulated opposite the measured wavelength. In most of these cases it is by no means certain which of the possible identified lines is present; one or the other may be, or both. On the other hand if a satellite line is possibly blended with one of the main-band lines, which are almost all much stronger, we did not attempt to measure the wavelength but entered "blend" in that column, and then gave both the main-band line and the satellite line in the other two columns. Again, it is by no means certain that the satellite line is present, but neither is it possible to rule it out.

TABLE 5
Wavelengths of Observed OH Satellite Lines

Measured	Calculated	Identification	Measured	Calculated	Identification
6552.80	6552.83	6 - 1 $^{Q}R_{12}(0.5)$	7987.50	7987.53	5 - 1 $^{Q}R_{12}(1.5)$
6578.17	6578.15	6 - 1 $^{P}Q_{12}(1.5)$		7987.59	5 - 1 $^{Q}R_{12}(2.5)$
6591.67	6591.68	6 - 1 $^{P}Q_{12}(2.5)$	blend	7993.33	5 - 1 $P_1(3.5)$
6803.08	6803.09	7 - 2 $^{Q}P_{21}(1.5)$		7993.59	5 - 1 $^{Q}R_{12}(3.5)$
6921.41	6921.43	7 - 2 $^{Q}R_{12}(1.5)$	7994.03	7994.07	5 - 1 $^{Q}R_{12}(0.5)$
6924.59	6924.62	7 - 2 $^{Q}R_{12}(0.5)$	7998.12	7998.12	9 - 4 $^{O}P_{12}(4.5)$
6951.70	6951.71	7 - 2 $^{P}Q_{12}(1.5)$	8031.78	8031.80	5 - 1 $^{P}Q_{12}(1.5)$
6966.34	6966.35	7 - 2 $^{P}Q_{12}(2.5)$	8049.79	8049.90	5 - 1 $^{P}Q_{12f}(2.5)$
6986.12	6986.14	7 - 2 $^{P}Q_{12f}(3.5)$	8050.02	8050.16	5 - 1 $^{P}Q_{12e}(2.5)$
6986.37	6986.35	7 - 2 $^{P}Q_{12e}(3.5)$	8074.38	8074.42	5 - 1 $^{P}Q_{12f}(3.5)$
7207.88	7207.87	8 - 3 $^{Q}P_{21}(1.5)$	8074.71	8074.74	5 - 1 $^{P}Q_{12e}(3.5)$
7225.22	7225.19	8 - 3 $^{Q}P_{21}(2.5)$	8094.95	8094.99	5 - 1 $^{O}P_{12}(2.5)$
7341.67	7341.74	8 - 3 $^{Q}R_{12}(1.5)$	8138.36	8138.39	5 - 1 $^{O}P_{12}(3.5)$
7344.91	7344.93	8 - 3 $^{Q}R_{12}(0.5)$	8255.19	8255.13	6 - 2 $^{Q}P_{21}(1.5)$
7374.07	7374.09	8 - 3 $^{P}Q_{12}(1.5)$	8427.50	8427.52	6 - 2 $^{Q}R_{12}(1.5)$
7390.11	7390.12	8 - 3 $^{P}Q_{12}(2.5)$		8427.76	6 - 2 $^{Q}R_{12}(2.5)$
7411.84	7411.88	8 - 3 $^{P}Q_{12f}(3.5)$	8434.39	8434.43	6 - 2 $^{Q}R_{12}(0.5)$
7412.05	7412.10	8 - 3 $^{P}Q_{12e}(3.5)$		8434.48	6 - 2 $^{Q}R_{12}(3.5)$
7422.86	7422.90	8 - 3 $^{O}P_{12}(2.5)$	8474.63	8474.66	6 - 2 $^{P}Q_{12}(1.5)$
7458.36	7458.38	8 - 3 $^{O}P_{12}(3.5)$	8494.07	8494.07	6 - 2 $^{P}Q_{12f}(2.5)$
7499.71	7499.74	8 - 3 $^{O}P_{12}(4.5)$	8494.30	8494.34	6 - 2 $^{P}Q_{12e}(2.5)$
7546.48	7546.57	8 - 3 $^{O}P_{12f}(5.5)$	8520.40	8520.46	6 - 2 $^{P}Q_{12f}(3.5)$
7546.83	7546.90	8 - 3 $^{O}P_{12e}(5.5)$	8520.74	8520.79	6 - 2 $^{P}Q_{12e}(3.5)$
7590.09	7590.08	4 - 0 $^{Q}R_{12}(2.5)$	8542.08	8542.09	6 - 2 $^{O}P_{12}(2.5)$
	7590.10	4 - 0 $^{Q}R_{12}(1.5)$	8553.14	8553.17	6 - 2 $^{P}Q_{12f}(4.5)$
7672.86	7672.84	9 - 4 $^{Q}P_{21}(1.5)$	8553.51	8553.55	6 - 2 $^{P}Q_{12e}(4.5)$
7692.30	7692.26	9 - 4 $^{Q}P_{21}(2.5)$	blend	8693.20	7 - 3 $^{R}Q_{21}(1.5)$

In Table 6 we have listed in condensed form all the satellite OH lines we have observed in our night-sky spectra. We could detect none at the shortest wavelengths, where $\nu' - \nu''$ is large, and consequently even the main OH bands are weak. Because of the much better signal-to-noise ratio spectra we have at medium wavelengths (due to the decreasing sensitivity of the CCD at longer wavelengths, and also the shorter exposure times for the spectra reported in this Paper II), most of the identified satellite lines are in this region. But in addition, note that the bands of lowest vibrational quantum numbers, such as $(4 - 0)$ and $(5 - 1)$, tend to have weaker satellite lines than the bands with higher vibrational quantum number which are near them in wavelength. The bands with lower vibrational quantum number $\nu'' = 0$ are weakest of all; no $(5 - 0)$ satellite lines were detected. Within a given satellite band only rotational lines of low J have been detected; they are the strongest lines, just as in the main bands. No $^{S}R_{21}$ lines and only a very few $^{R}Q_{21}$ lines have been detected; they are evidently the weakest satellite bands.

Note the feature measured at λ8427.50 is clearly largely $(6 - 2)$ $^{Q}R_{12}(1.5)$ λ8427.52; $(6 - 2)$ $^{Q}R_{12}(2.5)$ λ8427.76 is not resolved from it at all and must be considerably fainter, but the profile is somewhat broadened and asymmetrical toward longer wavelength, indicating it is probably weakly present. Also, as Table 6 shows, the only satellite band for which we detected lines but did not detect the line of lowest possible J'' is $(4-0)$ $^{Q}R_{12}$. For it, $^{Q}R_{12}(0.5)$ λ7596.26 is definitely not present on our spectra.

7. CORRECTIONS

In our Paper I, Fig. 1 of order 49, the two lines $(7 - 2)$ $P_{2f,e}$ (12.5) are incorrectly labeled. The wavelengths given there, λλ7336.944, 7337.861 should read λλ7346.944, 7347.861. This was a misprint in the labeling; the wavelengths are correctly given in Table 2 of that paper and in the supplemental table. Also, the possible identification of weak [C I] λ8727.13 given in Sec. 5 of that paper is incorrect; the wavelength discrepancy is far too large to be a measuring error, even for a weak line. We now realize that

TABLE 6
Observed J'' of Satellite OH Bands

$v'-v''$	$^{Q}R_{12}$	$^{P}Q_{12}$	$^{O}P_{12}$	$^{Q}P_{21}$	$^{R}Q_{21}$
6 - 1	0.5	1.5, 2.5	-	-	-
7 - 2	0.5, 1.5	1.5, 2.5, 3.5	-	1.5	-
8 - 3	0.5, 1.5	1.5, 2.5, 3.5	2.5, 3.5, 4.5, 5.5	1.5, 2.5	-
9 - 4	0.5, 1.5	1.5b, 2.5, 3.5, 4.5	2.5b, 3.5, 4.5	1.5. 2.5	-
4 - 0	1.5b, 2.5b	-	-	-	-
5 - 1	0.5, 1.5b, 2.5b, 3.5b	1.5, 2.5, 3.5	2.5, 3.5	1.5, 2.5	-
6 - 2	0.5, 1.5	1.5, 2.5, 3.5, 4.5	2.5	1.5	-
7 - 3	0.5, 1.5, 2.5	1.5, 2.5	2.5, 3.5, 4.5	1.5, 2.5, 3.5	1.5b, 2.5
8 - 4	-	1.5	-	-	-

b = blended and therefore not certainly present

the observed feature, with wavelength λ8726.70, is in fact the OH satellite line $(7 - 3)\ ^{Q}P_{21}(1.5)$, as listed in Table 6.

8. CONCLUSION

For convenience of use, the tables and figures from this paper are available via the WWW (http://www.ucolick.org/~jfulb/OH.html). The figures are available in PostScript form, while the tables are available in PostScript, Latex, and ASCII form. There is one supplemental table which expands our previous one, made available after publication of Paper I. This supplemental table expands Table 2 of Paper I and of the present paper to include the wavelengths of the lines already published by Abrams et al. (1994).

We are most grateful to Peter Gillingham, the director of operations of the W. M. Keck Observatory for allowing one of us (T.A.B.) to obtain sky spectra in the longer-wavelength CCD region, as yet little used by high-resolution astronomical spectroscopists, for inclusion in this paper. We are grateful to Steven S. Vogt and Joseph S. Miller for their encouragement and assistance in getting and using the Keck HIRES data. We are particularly grateful to Robert P. Lowe and Gary Burns, for bringing the problem of identifying the OH satellite lines to our attention, emphasizing their importance, and informing us of their earlier work in these directions, and to Richard A. Copeland for drawing several important references to our attention. Finally, we wish to thank the National Science Foundation for partial support of this research under Grant AST 91-23547.

REFERENCES

Abrams, M. C., Davis, S. P., Rao, M. L. P., Engleman, R., Jr., and Brault, J. W. 1994, ApJS, 93, 351
Delbouille, L., Roland, G., and Neven, L. 1973, Atlas Photométrique du Spectre Solaire, Volume Special, Institut d'Astrophysique de l'Université de Liège
Dodd, J. A., Lipson, S. J., Lowell, J. R., Armstrong, P. S., Blumberg, W. A. M., Nadile, R. M., Adler-Gordon, S. M., Marinelli, W. J., Holtzclaw, K. W., and Green, B. D. 1994, J. Geophys. Res., 99, 3559
Edlén, B. 1953, JOSA, 43, 339
Edlén, B. 1966, Metrologia, 2, 71
Espy, P. H., and Hammond, M. R. 1955, J. Quant. Spectrosc. Radiat. Transf., 54, 879
Greet, P. A., French, W. J. R., Burns, G. B., Williams, P. F. B., and Lowe, R. P. 1997, Annales Geophysicae, submitted
Greet, P. A., Innes, J., and Dyson, P. L. 1994, Geophys. Res. Lett., 21, 1153
Herzberg, G. 1950, Molecular Spectra and Molecular Structure. I. Spectra of Diatomic Molecules (New York, Van Nostrand)
Krassovsky, V. L., Sherov, N. N., and Yarin, V. I. 1961, J. Atmos. Terr. Phys., 21, 46
Krassovsky, V. L., Sherov, N. N., and Yarin, V. I. 1962, Planet. Space. Sci., 9, 883
Moore, C. E., Minnaert, M. G. J., and Houtgast, J. 1966, The Solar Spectrum 2935 Å to 8770 Å, National Bureau of Standards, Monograph 61
Osterbrock, D. E., Fulbright, J. P., Martel, A. R., Keane, M. J., Trager, S. C., and Basri, G. 1996, PASP, 108, 277 (Paper I)
Pendleton, W., Espy, P., Baker, D., Steed, D., and Fetrow, M. 1989, J. Geophys. Research, 94, 505
Rees, M. H. 1989, Physics and Chemistry of the Upper Atmosphere (Cambridge, Cambridge University Press)
Taylor, M. J., Lowe, R. P., and Baker, D. J. 1995, Ann. Geophys., 13, 1116
Turnbull, D. N., and Lowe, R. P. 1983, Can. J. Phys., 61, 244
Vogt, S. 1987, PASP, 99, 1214
Vogt, S. et al., 1994, SPIE Conf. 2198, 361
Williams, P. F. B. 1996, Planet. Space Sci., 44, 163